Articles

Electrophilic Additions of Mercury and Gold Species to the Anion Carbide Cluster $[Fe_5C(CO)_{14}]^{2-}$. X-ray Crystal Structures of $(NEt_4)[Fe_5C(CO)_{14}\{\mu\text{-}HgW(CO)_3Cp\}]$ and $(NEt_4)_2[\mu_4\text{-}Hg\{Fe_5C(CO)_{14}\}_2]$

Roser Reina,[†] Olga Riba,[†] Oriol Rossell,[†] Miquel Seco,*[,†] Pilar Gómez-Sal,[‡] Avelino Martín,[‡] Dominique de Montauzon,[§] and Alain Mari[§]

Departament de Química Inorgànica, Universitat de Barcelona, Martí i Franquès, 1-11, E-08028 Barcelona, Spain, Departamento de Química Inorgánica, Universidad de Alcalá, E-28871 Alcalá de Henares, Spain, and Laboratoire de Chimie de Coordination du CNRS, 205 route de Narbonne, F-31077 Toulouse Cedex, France

Received March 5, 1998

The reaction of the carbide carbon anion $[Fe_5C(CO)_{14}]^{2-}$ with ClHgM in tetrahydrofuran gives the new heptametallic clusters $(NEt_4)[Fe_5C(CO)_{14}\{\mu\text{-}HgM\}]$ (M = $Mo(CO)_3Cp$ (**1a**), $W(CO)_3Cp$ (**1b**), $Mn(CO)_5$ (**1c**), $Co(CO)_4$ (**1d**), $Fe(CO)_2Cp$ (**1e**)). The spiro species $(NEt_4)_2[\mu_4\text{-}Hg\{Fe_5C(CO)_{14}\}_2]$ (**2**) has been isolated by reaction of the pentairon carbide carbon dianion with $Hg(NO_3)_2$. The structures of **1b** and **2** have been determined by X-ray diffraction methods. The anion of **1b** has an Fe_5 square-pyramidal metal skeleton in which a basal edge is bridged by the $HgW(CO)_3Cp$ moiety. For the cluster anion **2**, the metal core consists of a four-coordinate mercury atom bridging the bond edges of two square-based-pyramidal pentairon units. The electrochemical behavior of these compounds has been investigated by cyclic voltammetry and coulometry. The ^{57}Fe Mössbauer spectroscopy of complexes **1b**,**e** reveals the existence of three and four types of iron sites, respectively. This study has been extended by reacting the new species $(NEt_4)[Fe_5C(CO)_{14}\{\mu\text{-}HgM\}]$ (**1a**,**b**) with $AuPPh_3^+$ to give the neutral octametallic clusters $[Fe_5C(CO)_{14}\{\mu\text{-}HgM\}\{\mu\text{-}AuPPh_3\}]$ (M = $Mo(CO)_3Cp$ (**3a**), $W(CO)_3Cp$ (**3b**)).

Introduction

Although reactions between anionic carbonyl clusters and neutral or cationic metal fragments have been extensively investigated, the nature of the resulting products is not easily predicted if high-nuclearity anions are used. This is particularly true for metal anions containing a p-block element in an exposed semi-interstitial site, because of the option the incoming ligands have of interacting with either the metals or the main-group-atom sites.[1] As an example of this, we have recently described that the attachment of the isolobal species H^+, $AuPPh_3^+$, and $HgMo(CO)_3Cp^+$ to the $[Fe_4C(CO)_{12}]^{2-}$ anion occurs through different edges of the butterfly Fe_4C skeleton, producing, as a result, three skeletal cluster isomers.[2] The different site preferences of the isolobal fragments versus the butterfly anion $[Fe_4C(CO)_{12}]^{2-}$ have been explained on the basis of a theoretical study of the bonding capabilities of the iron anion and the three cationic species.[3] To extend our studies to higher nuclearity iron anions, in this paper we report the reaction of HgM^+ (M = a metal fragment) with the pentanuclear anion $[Fe_5C(CO)_{14}]^{2-}$ and the study of the reactivity of the newly generated complexes in the presence of electrophilic metal fragments.

Results and Discussion

The reaction of ClHgM with $(NEt_4)_2[Fe_5C(CO)_{14}]$ in THF at −5 °C afforded good yields of the reddish complexes $(NEt_4)[Fe_5C(CO)_{14}\{\mu\text{-}HgM\}]$ (M = $Mo(CO)_3Cp$ (**1a**), $W(CO)_3Cp$ (**1b**), $Mn(CO)_5$ (**1c**), $Co(CO)_4$ (**1d**), $Fe(CO)_2Cp$ (**1e**)).

1a−**e** are air-stable, but their THF solutions decompose slowly under nitrogen at room temperature. They were characterized by elemental analyses and spectroscopic techniques. The ν(CO) IR patterns show, together with the bands due to the M fragments, other bands of the $Fe_5C(CO)_{14}$ unit that are slightly shifted up about 40 cm^{-1}, which indicates a decrease in electron density in the iron atoms. The ^{13}C NMR spectra

[†] Universitat de Barcelona.
[‡] Universidad de Alcalá.
[§] Laboratoire de Chimie de Coordination du CNRS.

(1) Thimmappa, B. H. S. *Coord. Chem. Rev.* **1995**, *143*, 1.
(2) Reina, R.; Riba, O.; Rossell, O.; Seco, M.; Gómez-Sal, P.; Martín, A. *Organometallics* **1997**, *16*, 5113.
(3) Reina, R.; Rossell, O.; Seco, M.; Segalés, G. *An. Quim. Int. Ed.* **1998**, *94*, 9.

S0276-7333(98)00160-5 CCC: $15.00
Publication on Web 08/15/1998

Scheme 1

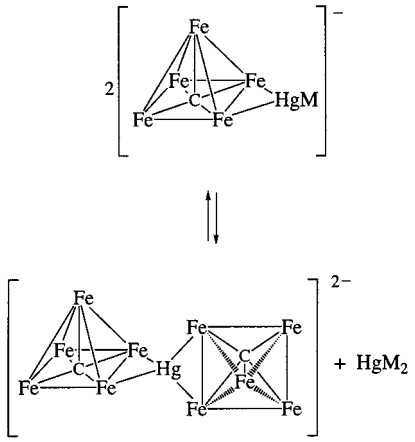

showed, along with the signals typical for carbonyl and C_5H_5 groups, the presence of the signal corresponding to the carbido carbon atom at very low fields (about 480 ppm). When **1a**−**e** were treated under electrospray mass spectrometry (ESMS) and fast atom bombardment mass spectrometry (FABMS) conditions, the patterns in all these spectra were similar and consisted of the parent molecular ion in high abundance along with those originated from the gradual loss of CO ligands. In addition, peaks due to the $[M - Hg(CO)_n]^-$ species were observed in all cases. The presence of these ions in the spectra can be understood as a demercuriation process of the parent anion, giving the corresponding $[Fe_5C(CO)_{14}\{M\}]^-$ anions. Moreover, complex **1e** is the most resistant to the Hg−M fragmentation, as has been reported for the series of anions $[Fe_3(CO)_{11}\{\mu\text{-HgM}\}]^-$ and $[Fe_4C(CO)_{12}\{\mu\text{-HgM}\}]^-$.[2,4] This fact may be attributed to the more nucleophilic character of the Fe(CO)$_2$Cp fragment as compared with the other M fragments. According to the spectroscopic data, the geometry of clusters **1a**−**e** was predicted as consisting of an Fe_5 square-pyramidal metal skeleton in which a basal edge is bridged by the mercury atom of the HgM^+ moiety. An alternative description in which the mercury atom occupies the sixth vertex of an Fe_5Hg octahedron seems less probable, since this geometry would force the mercury atom to adopt five-coordination, which is rare in its chemistry. A single-crystal X-ray study of compound **1b** has confirmed the proposed structure.

Curiously, during the process of the formation of **1a**−**e**, the IR spectra of the crude reaction solutions showed, in some cases, the presence of a medium-intensity band at 2038 cm^{-1}. However, with the use of an excess of the mercury compound, this effect was reduced. Given the known tendency of the mercury-containing clusters to undergo metal−ligand redistribution reactions in solution, we thought that this band might belong to the cluster $(NEt_4)_2[\mu_4\text{-Hg}\{Fe_5C(CO)_{14}\}_2]$, which would result from the process given in Scheme 1.

This symmetrization reaction is the usual one for neutral mercury compounds but is less favored for the anionic species since the presence of negative charge stabilizes them.[5] This is because such a process is known to proceed through an associative mechanism, which operates with difficulty with charged species.[6] Here, the probable delocalization of the charge over the seven metal atoms of the clusters cannot avoid the approach of the reactants to promote a partial ligand redistribution. To confirm this hypothesis, we undertook the synthesis of $(NEt_4)_2[\mu_4\text{-Hg}\{Fe_5C(CO)_{14}\}_2]$ (**2**) by allowing $Hg(NO_3)_2$ to react with $(NEt_4)_2[Fe_5C(CO)_{14}]$ in THF at room temperature. **2** was obtained as a red crystalline solid in 60% yield. Its IR spectrum in the ν(CO) region confirmed the presence of the band at 2038 cm^{-1}. The mass spectra show the peaks attributable to $[M + H]^-$ and $[M + NEt_4]^-$ species, apart from those corresponding to the gradual loss of CO ligands and mercury. Interestingly, by ESMS it is also possible to observe the $M/2$ peak. It is worth noting that in the ^{13}C NMR spectrum two signals at 482.3 and 480.8 ppm assignable to carbon carbide atoms were present, suggesting that the two metal units are not identical in solution. According to the spectroscopic data the more plausible metal skeleton of **2** is thought to be formed by two Fe_5C square-pyramidal units edge-bridged by a mercury atom in a μ_4 bonding mode. This structure was confirmed by X-ray analysis.

Description of the Crystal Structure of $(NEt_4)[Fe_5C(CO)_{14}\{\mu\text{-HgW(CO)}_3\text{Cp}\}]$ (1b). In the crystals of **1b**, NEt_4^+ cations and $[Fe_5C(CO)_{14}\{\mu\text{-HgW(CO)}_3\text{Cp}\}]^-$ anions are present. The structure of the anion is shown in Figure 1, together with the atomic numbering scheme. Selected bond distances and angles are listed in Table 1. The basic skeleton consists of a distorted Fe_5 square-based pyramid where an Fe−Fe bond of a basal edge is bridged by the HgW(CO)$_3$Cp fragment. The attachment of the mercury species to the $[Fe_5C(CO)_{14}]^{2-}$ anion promotes a rearrangement of the carbonyl ligands, and thus, three of them appear as bridging the three remaining basal edges in **1b** instead of the two bridging carbonyl ligands found in the starting anion.[7] As expected, the mercury coordination to the Fe(1)−Fe(4) edge causes an appreciable lengthening in the distances between these iron atoms (2.898 Å). On the other hand, the Fe(apical)−Fe(basal) bond lengths are significantly larger (mean 2.63 Å) than those between basal Fe atoms (mean 2.57 Å), ignoring the Fe(1)−Fe(4) edge. The geometry around mercury is roughly trigonal planar. The two W−Hg−Fe angles are 147.43 and 145.79°, and the mercury atom only lies 0.144 Å above the plane defined by the Fe atoms bonded to it and the W atom. The HgW(CO)$_3$Cp moiety shows the usual "four-legged piano stool" arrangement with a W−Hg distance of 2.762 Å. The carbide atom is located below the iron basal mean plane, the distance from this plane being 0.13 Å, which lies between that found for the clusters $[Fe_5C(CO)_{15}]$ (0.09 Å) and $[Fe_5C(CO)_{14}]^{2-}$ (0.18 Å). This distance is a measure of the negative charge on the carbon carbide atom.[8] This feature has also been observed for the homologous osmium clusters $[Os_5C(CO)_{15}]$ and $[Os_5C(CO)_{14}]^{2-}$ as well as for the series of

(4) Ferrer, M.; Reina, R.; Rossell, O.; Seco, M.; Segalés, G. *J. Organomet. Chem.* **1996**, *515*, 205.

(5) Reina, R.; Rossell, O.; Seco, M. *J. Organomet. Chem.* **1990**, *398*, 285.

(6) Abraham, M. H. In *Comprehensive Chemical Kinetics*; Bamford, C. H., Tipper, C. F. H., Eds.; Elsevier: Amsterdam, 1973; Vol. 12.

(7) Gourdon, A.; Jeannin, Y. *J. Organomet. Chem.* **1985**, *290*, 199.

(8) Withmire, K. H. *J. Coord. Chem.* **1988**, *17*, 95.

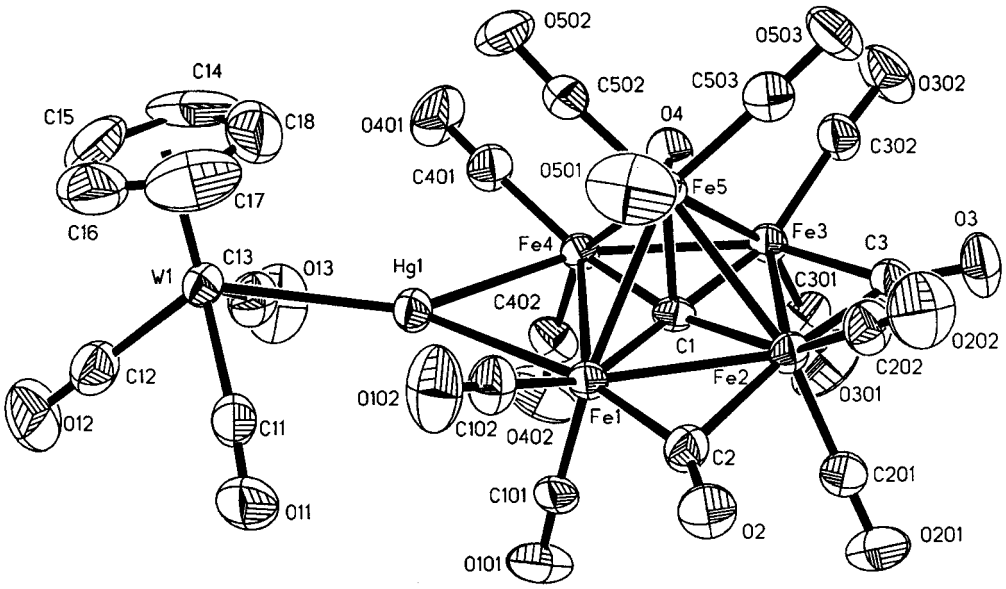

Figure 1. View of the molecular structure of the cluster anion $[Fe_5C(CO)_{14}\{\mu\text{-}HgW(CO)_3Cp\}]^-$ (anion of **1b**) together with the atomic numbering scheme.

Table 1. Selected Bond Lengths (Å) and Angles (deg) for 1b

Hg(1)−Fe(1)	2.669(1)	Fe(3)−Fe(4)	2.555(2)
Hg(1)−Fe(4)	2.682(2)	Fe(3)−Fe(5)	2.633(2)
Hg(1)−W(1)	2.762(1)	Fe(4)−Fe(5)	2.626(2)
Fe(1)−Fe(2)	2.580(2)	Fe(1)−C(1)	1.867(8)
Fe(1)−Fe(4)	2.898(2)	Fe(2)−C(1)	1.885(8)
Fe(1)−Fe(5)	2.639(2)	Fe(3)−C(1)	1.894(8)
Fe(2)−Fe(3)	2.566(2)	Fe(4)−C(1)	1.880(8)
Fe(2)−Fe(5)	2.608(2)	Fe(5)−C(1)	1.967(8)
Fe(1)−Hg(1)−Fe(4)	65.59(4)	Fe(3)−Fe(4)−Fe(1)	86.57(6)
Fe(1)−Hg(1)−W(1)	147.43(3)	Hg(1)−Fe(4)−Fe(1)	56.98(4)
Fe(4)−Hg(1)−W(1)	145.79(3)	Fe(1)−C(1)−Fe(5)	86.9(3)
Fe(2)−Fe(1)−Fe(4)	86.00(6)	Fe(4)−C(1)−Fe(5)	86.1(3)
Hg(1)−Fe(1)−Fe(4)	57.43(5)	Fe(2)−C(1)−Fe(5)	85.2(3)
Fe(3)−Fe(2)−Fe(1)	93.47(6)	Fe(3)−C(1)−Fe(5)	85.9(3)
Fe(4)−Fe(3)−Fe(2)	93.94(6)		

ruthenium derivatives $[Ru_5C(CO)_{15-x}(PPh_3)_x]$.[9−11] The average distance between the carbide and the basal iron atoms is 1.88 Å, appreciably shorter than that of 1.967 Å observed for C−Fe_5(apical).

Description of the Crystal Structure of $(NEt_4)_2$-$[\mu_4$-Hg$\{Fe_5C(CO)_{14}\}_2]$ (2). The structure of the cluster anion of **2** is depicted in Figure 2 together with the atomic numbering system; the main bond distances and angles are given in Table 2. The structure reveals a four-coordinate mercury atom bridging the basal edges of two square-based-pyramid pentairon units. The dihedral angle between the two Fe_2Hg planes is 81.2-(1)°. Consequently, the coordination geometry around mercury can be described roughly as tetrahedral. To our knowledge, the value of the dihedral angle is the highest described for this type of spiro derivative. For instance, for the compounds $[\mu_4$-Hg$\{Fe_2Co(CO)_7(\mu_3$-COMe)Cp$\}_2]$, $[\mu_4$-Hg$\{Fe_2(CO)_6(\mu$-^{t}BuS)$(\mu$-CH_3OCH_2CH═C)$\}_2]$, and $[\mu_4$-Hg$\{Ru_6C(CO)_{16}\}_2]^{2-}$ values of 46.4, 35.5, and 73.7° were reported, respectively, and can be correlated with the steric congestion of the molecule.[12−14] Interestingly, the observed nonequivalence of the two $Fe_5C(CO)_{14}$ units, as evidenced by ^{13}C NMR spectroscopy, is confirmed in the solid state. Thus, the angles Fe(4)−Hg(1)−Fe(1) and Fe(7)−Hg(1)−Fe(6) present a difference of 0.5°. As expected, each square-based-pyramidal unit displays three carbonyl ligands bridging three basal edges while the fourth is bridged by the mercury atom; bond distances and angles for **2** are similar to those found for **1b**.

Structural Comparison of 1b and the Homologous Iron/Gold Cluster. The homologous gold cluster of **1b**, $[Fe_5C(CO)_{14}\{AuPEt_3\}]^-$, is reported in the literature, which was obtained by reacting $[Fe_5C(CO)_{14}]^{2-}$ with an equimolar amount of $ClAuPEt_3$.[15] The compound was not isolated, and from its unique reported data, the infrared carbonyl stretching frequencies of its solution, it was not possible to ascertain the site attachment of the gold atom. Fortunately, the X-ray crystal structure of the neutral cluster, $[Fe_5C(CO)_{14}$-$(AuPEt_3)_2]$, obtained by using an excess of the gold derivative, revealed a metal core based on an iron square-based pyramid. Linked to this, two $AuPEt_3$ groups were found to display different bonding modes: one bridges a basal edge while the other caps the square base of the Fe_5 square pyramid to give a distorted-spiked-octahedral metal arrangement. What remained unclear was the site attachment of the gold unit in $[Fe_5C(CO)_{14}\{AuPEt_3\}]^-$. In other words, which is the preferred site attachment of the first incoming gold fragment?. Recently, we allowed the iron cluster to react successively with 1 and 2 mol of $ClAuPPh_3$, the

(9) Johnson, B. F. G.; Lewis, J.; Nelson, W. J. H.; Nicholls, J. N.; Puga, J.; Raithby, P. R.; Rosales, M. J.; Schroder, M.; Vargas, M. D. *J. Chem. Soc., Dalton Trans.* **1983**, 2447.
(10) Johnson, B. F. G.; Lewis, J.; Nicholls, J. N.; Puga, J.; Raithby, P. R.; Rosales, M. J.; McPartlin, M.; Clegg, W. *J. Chem. Soc., Dalton Trans.* **1983**, 277.
(11) Farrar, D. H.; Jackson, P. F.; Johnson, B. F. G., Lewis, J.; Nicholls, J. N.; McPartlin, M. *J. Chem. Soc., Chem. Commun.* **1981**, 415.
(12) Farrugia, L. J. *J. Chem. Soc., Chem. Commun.* **1987**, 147.
(13) Seyferth, D.; Ruschke, D. P.; Davis, W. M.; Cowie, M.; Hunter, A. D. *Organometallics* **1994**, *13*, 3834.
(14) Johnson, B. F. G.; Whei-Lu, K.; Lewis, J.; Raithbay, P. R.; Saharan, V. P. *J. Chem. Soc., Dalton Trans.* **1991**, 1037.
(15) Johnson, B. F. G.; Kaner, D. A.; Lewis, J.; Rosales, M. J. *J. Organomet. Chem.* **1982**, *238*, C73.

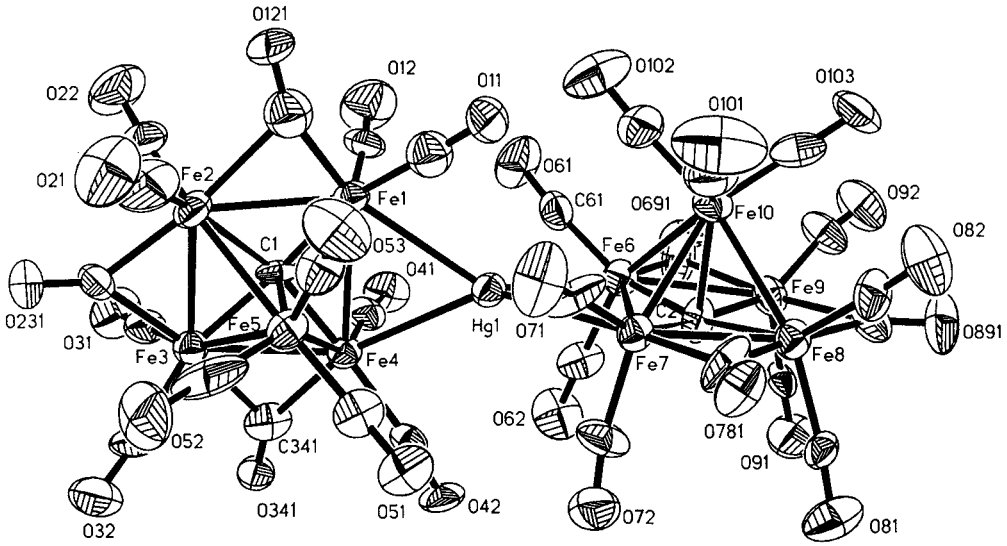

Figure 2. View of the molecular structure of the cluster anion $[\mu_4\text{-Hg}\{Fe_5C(CO)_{14}\}_2]^{2-}$ (anion **2**) together with the atomic numbering scheme.

Table 2. Selected Bond Lengths (Å) and Angles (deg) for 2

Hg(1)−Fe(1)	2.756(3)	Fe(7)−Fe(8)	2.570(4)
Hg(1)−Fe(4)	2.724(3)	Fe(7)−Fe(10)	2.616(4)
Hg(1)−Fe(6)	2.732(3)	Fe(8)−Fe(9)	2.557(4)
Hg(1)−Fe(7)	2.721(3)	Fe(8)−Fe(10)	2.574(4)
Fe(1)−Fe(2)	2.572(4)	Fe(9)−Fe(10)	2.656(4)
Fe(1)−Fe(4)	2.877(4)	Fe(1)−C(1)	1.83(2)
Fe(1)−Fe(5)	2.625(4)	Fe(2)−C(1)	1.91(2)
Fe(2)−Fe(3)	2.559(4)	Fe(3)−C(1)	1.93(2)
Fe(2)−Fe(5)	2.583(4)	Fe(4)−C(1)	1.87(2)
Fe(3)−Fe(4)	2.572(4)	Fe(5)−C(1)	1.99(2)
Fe(3)−Fe(5)	2.635(4)	Fe(6)−C(2)	1.90(2)
Fe(4)−Fe(5)	2.635(4)	Fe(7)−C(2)	1.85(2)
Fe(6)−Fe(7)	2.883(4)	Fe(8)−C(2)	1.87(2)
Fe(6)−Fe(9)	2.575(4)	Fe(9)−C(2)	1.90(2)
Fe(6)−Fe(10)	2.639(4)	Fe(10)−C(2)	1.99(2)
Fe(4)−Hg(1)−Fe(1)	63.33(8)	Hg(1)−Fe(6)−Fe(7)	57.90(8)
Fe(6)−Hg(1)−Fe(1)	138.39(9)	Fe(8)−Fe(7)−Fe(6)	86.6(1)
Fe(7)−Hg(1)−Fe(1)	136.79(9)	Hg(1)−Fe(7)−Fe(6)	58.28(8)
Fe(7)−Hg(1)−Fe(4)	140.95(9)	Fe(9)−Fe(8)−Fe(7)	93.4(1)
Fe(7)−Hg(1)−Fe(6)	63.82(8)	Fe(8)−Fe(9)−Fe(6)	93.8(1)
Fe(4)−Hg(1)−Fe(6)	128.91(9)	Fe(1)−C(1)−Fe(5)	86.7(6)
Fe(2)−Fe(1)−Fe(4)	86.6(1)	Fe(4)−C(1)−Fe(5)	85.9(7)
Hg(1)−Fe(1)−Fe(4)	57.80(8)	Fe(3)−C(1)−Fe(5)	84.4(7)
Fe(3)−Fe(2)−Fe(1)	93.3(1)	Fe(2)−C(1)−Fe(5)	82.8(7)
Fe(2)−Fe(3)−Fe(4)	93.8(1)	Fe(7)−C(2)−Fe(10)	85.9(7)
Fe(3)−Fe(4)−Fe(1)	86.2(1)	Fe(8)−C(2)−Fe(10)	83.5(7)
Hg(1)−Fe(4)−Fe(1)	58.87(8)	Fe(9)−C(2)−Fe(10)	86.0(9)
Fe(9)−Fe(6)−Fe(7)	86.1(1)	Fe(6)−C(2)−Fe(10)	85.3(9)

reaction being monitored by ^{31}P NMR spectroscopy.[16] The first signal appeared at 32.5 ppm, but after the addition of a second equivalent of $ClAuPPh_3$ a new signal at 55.7 ppm appeared. This latter signal lies in the same range expected for those compounds containing the $AuPPh_3$ moiety bonded in a μ_2 manner. Consequently, the signal at about 32 ppm should correspond to a μ_4-$AuPPh_3$ group, so we can conclude that the first incoming gold group caps the square base of the pyramid while the second should bridge one of the basal edges of the iron skeleton.

On the other hand, the reaction of the proton toward the dianionic iron carbonyl cluster was also explored. Thus, treatment of $(NEt_4)_2[Fe_5C(CO)_{14}]$ with HCl quantitatively yielded the unstable $(NEt_4)[HFe_5C(CO)_{14}]$.[17] Although there are no data available for this compound, the protonation seems to occur on the iron skeleton and not on the carbide, as observed for the alkylated species $[Fe_5C(CO)_{13}(\mu\text{-}COCH_3)]^-$, which exhibits a metal skeleton identical with that of the starting iron anion and is able to add a proton in an edge-bridging bonding mode, according to the ^1H NMR spectrum. Moreover, very simple extended Hückel results carried out on Fe_nC and $(HFe)_nC$ (n = 5, 6) correlate with this lack of reactivity of the carbide carbon atom.[18]

In conclusion, despite the fact that H^+, $AuPPh_3^+$, and HgM^+ are isolobal species, the site preference toward the $[Fe_5C(CO)_{14}]^{2-}$ anion is not the same. Thus, while HgM^+ and H^+ prefer to bridge an edge of the basal square pyramid, $AuPPh_3^+$ tends to cap the square base.

In an attempt to rationalize the latter results, we undertook a theoretical study based on extended Hückel calculations of the bonding capability of the iron anion toward HgM^+ and $AuPPh_3^+$ fragments. The simplest way to study the bonding consists of dissecting the species $[Fe_5C(CO)_{14}\{\mu\text{-}HgW(CO)_3Cp\}]^-$ into two fragments, $[Fe_5C(CO)_{14}]^{2-}$ and $HgW(CO)_3Cp^+$, seeing how they interact, and comparing with the results obtained for the hypothetical $[Fe_5C(CO)_{14}\{\mu\text{-}AuPPh_3\}]^-$. In both cases a strong σ bond and a very weak π interaction are found to occur, the mercury cluster being somewhat more stable than the gold derivative. In the same way, we compared the hypothetical species $[Fe_5C(CO)_{14}\{\mu_4\text{-}HgW(CO)_3Cp\}]^-$ and $[Fe_5C(CO)_{14}\{\mu_4\text{-}AuPPh_3\}]^-$. Here, the μ_4 bonding interaction between the iron anion and the mercury or gold fragments is weaker than in the μ_2 attachment. In the case of the mercury cluster, this can be understood because the mercury orbitals bonding the iron anion are basically the same as those bonding the tungsten atom (a similar observation was found in the study of $[Fe_4C(CO)_{12}]^{2-}$ versus H^+, $HgMo(CO)_3Cp^+$, and $AuPPh_3^+$).[3] However, for the gold complex a noticeable interaction between the carbide p_z orbital and the gold

(16) Rossell, O.; Seco, M.; Segalés, G.; Pellinghelli, M. A.; Tiripicchio, A. *J. Organomet. Chem.*, in press.

(17) Tachikawa, M.; Muetterties, E. L. *J. Am. Chem. Soc.* **1980**, *102*, 4544.

(18) Kollis, J. W.; Basolo, F.; Shriver, D. F. *J. Am. Chem. Soc.* **1982**, *104*, 5626.

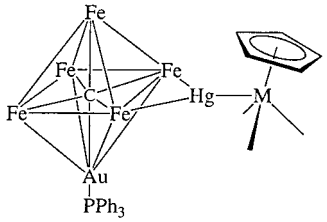

Figure 3.

sp_z hybrid orbital occurs. This would explain the tendency of the gold fragments to be incorporated in a μ_4 mode into the $[Fe_5C(CO)_{14}]^{2-}$ anion. However, it should be pointed out that the σ bond is weak, which agrees with the lack of reactivity at the carbide carbon atom mentioned above.

Synthesis of Au- and Hg-Containing Iron Clusters. The isolation of **1b** as well as the tendency of $AuPPh_3^+$ to cap the square base of the $[Fe_5C(CO)_{14}]^{2-}$ anion prompted us to try the formation of the mixed Au/Hg compound of the iron anion by treatment of **1a**,**b** with $ClAuPPh_3$. The reaction was instantaneous, and the shift of the ν(CO) IR bands to higher frequencies suggested that the gold fragment is, in fact, incorporated in the Fe_5Hg metal core. Workup of the CH_2Cl_2 solution allowed us to obtain brown crystals of the new neutral cluster $[Fe_5C(CO)_{14}\{HgM(CO)_3Cp\}\{AuPPh_3\}]$ (M = Mo (**3a**), W (**3b**)). These compounds were characterized by elemental analyses and spectroscopic techniques (see Experimental Section). The ^{31}P NMR spectrum shows a single signal at about 33 ppm, which confirms the μ_4-$AuPPh_3$ mode coordination. Accordingly, we propose the structure depicted in Figure 3 for **3a**,**b**, in which the Hg atom bridges a basal edge of the square pyramid while the gold atom caps the square Fe_4 base. Unfortunately, we have not been able to grow single crystals of **3a**,**b** because of their tendency to undergo decoordination in solution of the gold moiety, probably because of the strong steric congestion of the two voluminous metal fragments and the weakness of the μ_4-gold bond. To our knowledge, complexes **3a**,**b** represent the first example of metal−carbide clusters that simultaneously contain gold and mercury atoms.

Electrochemical Study of Compounds $(NEt_4)[Fe_5C(CO)_{14}\{\mu\text{-}HgM\}]$ (1a−e) and $(NEt_4)_2[\mu_4\text{-}Hg\{Fe_5C(CO)_{14}\}_2]$ (2). The electrochemical properties of the title compounds **1a**−**e** and **2** were studied in the electroactivity range of the solvent (CH_2Cl_2), to compare their electrochemical behavior with that of related systems. A cyclic voltammogram of $(NEt_4)[Fe_5C(CO)_{14}\{\mu\text{-}HgW(CO)_3Cp\}]$ (**1b**) is displayed in Figure 4a as representative of all compounds.

The voltammograms of the monoanionic compounds reveal three main electrode processes: (i) an irreversible oxidation wave around 0.8 V (I), (ii) a reduction wave around −0.8 V (IV) (the reversibility of the process depends on the scan rate), and (iii) a reversible reduction wave at −1.56 V (VI).

The waves II, III, and V are associated with the species $[Fe_6C(CO)_{16}]^{2-}$, formed in process IV. The electrochemical study of this cluster has been outlined elsewhere.[19]

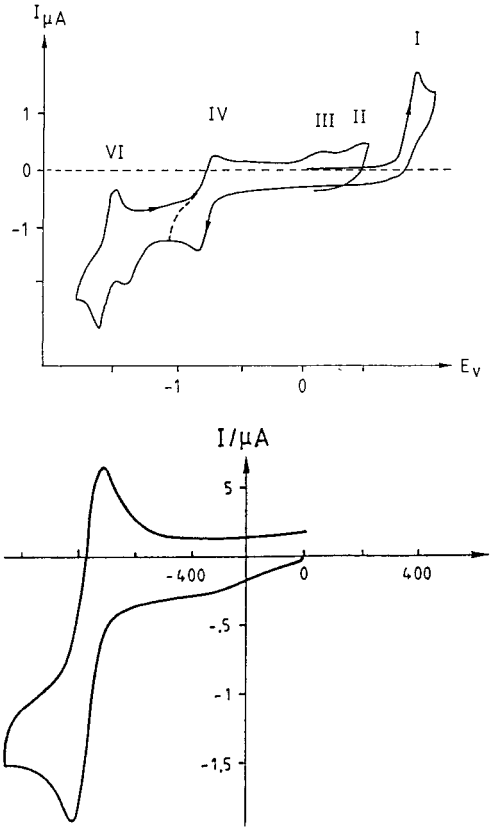

Figure 4. Ambient-temperature cyclic voltammograms of **1b** in CH_2Cl_2 measured at a platinum-bead electrode at a scan rate of 0.1 V s^{-1}: (a, top) full scan; (b, bottom) scan for the reversible reduction process (IV).

The electron-transfer rate constant k^0 determined by the Nicholson and Shain method using a Technic[20] ultramicroelectrode is approximately 10^{-2} cm s^{-2}, this value being typical of a quasi-reversible process.[21] The linear voltammograms at a rotating-Pt-disk electrode show a well-developed wave with the appearance of a slow electron transfer according to the nature of the electrode surface. We observed some passivation phenomena, especially when the potential sweeps over the whole electroactivity range. The study of the variation of the limiting currents as a function of the complex concentration, or as a function of the square root of the electrode rotation speed, shows a deviation from linearity for a diffusion-controlled process. Data for processes I, IV, and VI are summarized in Table 3.

Controlled-potential coulometry at +1.0 V required 1 faraday/mol and results in the formation of a neutral radical which decomposes further. We propose the mechanism shown in eqs 1 and 2.

$$[Fe_5C(CO)_{14}\{\mu\text{-}HgM\}]^- \rightleftharpoons [Fe_5C(CO)_{14}\{\mu\text{-}HgM\}]^\bullet + e^- \quad (1)$$

$$[Fe_5C(CO)_{14}\{\mu\text{-}HgM\}]^\bullet \rightarrow [Fe_5C(CO)_{15}] + \ldots \quad (2)$$

A controlled-potential electrolysis is run at −1.1 V, showing that one electron is exchanged for the reduction process IV. This wave appears reversible at ν = 0.1 V/s

(19) Rimmelin, J.; Lemoine, P.; Gross, M.; Mathieu, R.; de Montauzon, D. *J. Organomet. Chem.* **1986**, *309*, 355.

(20) (a) Nicholson, R. S. *Anal. Chem.* **1965**, *36*, 1351. (b) Nicholson, R. S.; Shain, I. *Anal. Chem.* **1966**, *37*, 706.

(21) Delahay, P. *J. Am. Chem. Soc.* **1953**, *75*, 1430.

Table 3. Electrochemical Processes for Compounds 1a−e and 2 in CH_2Cl_2 at 0.1 V/s[a]

compd	oxidn (I) $E_{p,a}$ (V)	redn (IV) $E^{o\prime}$ (V)	redn (IV) ΔE (mV)	redn (IV) $i_{p,a}/i_{p,c}$	redn (VI) $E^{o\prime}$ (V)	redn (VI) ΔE (mV)	redn (VI) $i_{p,a}/i_{p,c}$
1a	0.82	−0.80[b]	95[b]	0.82[b]	−1.56	72	0.85
1b	0.81	−0.80	79	0.94	−1.56	63	0.89
1c	0.81	−0.80[b]	90[b]	0.83[b]	−1.56	68	0.90
1d	0.80	−0.74[c]	110[c]	0.62[c]	−1.55	72	0.89
1e	0.80	−0.81[c]	101[c]	0.73[c]	−1.57	70	0.87
2	0.81	−0.81[d]	153[d]	0.53[d]	−1.56	65	0.86

[a] $n = 1$ in all cases. [b] $v = 0.3$ V/s. [c] $v = 1.5$ V/s. [d] $v = 1.0$ V/s.

if the potential sweep is restricted to the range of this electrochemical process for compound **1b** (Figure 4b). Otherwise, for complexes **1a** and **1c**, the reversibility appears at $v = 0.3$ V/s and for **1d** and **1e** at $v = 1.5$ V/s. These results could be rationalized according to an EC scheme: an electrode reaction (eq 3) (E), followed by a single chemical reaction (eq 4) (C).

$$\text{E: } [Fe_5C(CO)_{14}\{\mu\text{-HgM}\}]^- \underset{-e^-}{\overset{+e^-}{\rightleftharpoons}} [Fe_5C(CO)_{14}\{\mu\text{-HgM}\}]^{\bullet 2-} \quad (3)$$

$$\text{C: } [Fe_5C(CO)_{14}\{\mu\text{-HgM}\}]^{\bullet 2-} \rightarrow [Fe_6C(CO)_{16}]^{2-} + M^- + Hg + \ldots \quad (4)$$

The radical dianion formed in eq 3 is again reduced (process VI). We proposed an EC mechanism, where the chemical reaction generates the starting material, the M fragment, and free mercury (eqs 5 and 6).

$$\text{E: } [Fe_5C(CO)_{14}\{\mu\text{-HgM}\}]^{\bullet 2-} \underset{-e^-}{\overset{+e^-}{\rightleftharpoons}} [Fe_5C(CO)_{14}\{\mu\text{-HgM}\}]^{3-} \quad (5)$$

$$\text{C: } [Fe_5C(CO)_{14}\{\mu\text{-HgM}\}]^{3-} \rightarrow [Fe_5C(CO)_{14}]^{2-} + M^- + Hg \quad (6)$$

The nature of the decomposition products ($[Fe_5C(CO)_{15}]$, $[Fe_5C(CO)_{14}]^{2-}$, $[Fe_6C(CO)_{16}]^{2-}$, etc.) has been detected by IR spectroscopy and cyclic voltammetry studies.[19,22]

These data indicate the ease with which the Hg−M bond cleavage occurs during the electrochemical reduction, as found for the following mercury clusters: M_2Hg,[23] $(PPh_4)[Fe_3(CO)_{11}\{\mu\text{-HgM}\}]$,[24] $(PPh_4)[Mn_3(CO)_{12}(H)\{\mu\text{-HgM}\}]$,[25] $[Ru_3(CO)_9\{\mu\text{-HgMo(CO)}_3\text{Cp}\}(\mu_3\text{-}\eta^2\text{-C}{=}\text{C}^t\text{Bu})]$,[26] $(NEt_4)[Fe_6C(CO)_{16}\{\mu\text{-HgM}\}]$,[27] and $(PPh_4)[Fe_4C(CO)_{12}\{\mu\text{-HgM}\}]$.[2]

The cyclic voltammogram of $(NEt_4)_2[\mu_4\text{-Hg}\{Fe_5C(CO)_{14}\}_2]$ (**2**) is largely similar to those of **1a**−**e**. It exhibits one irreversible oxidation and two reduction processes. The first reduction becomes quasi-reversible at 1.0 V/s, while the reversibility of the second wave is not dependent on the scan rate. Data for these processes are summarized in Table 3.

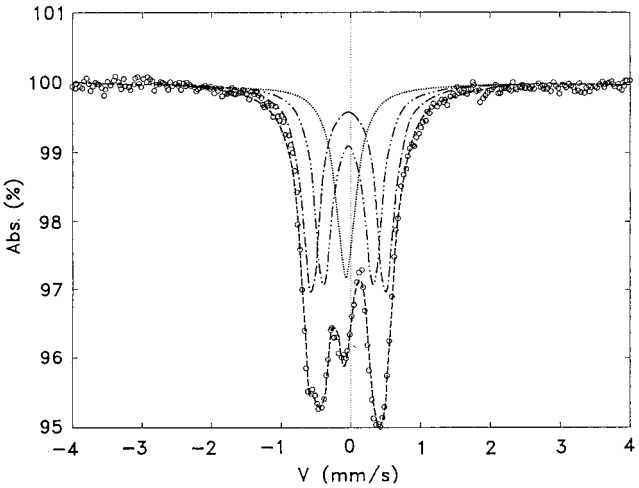

Figure 5. ^{57}Fe Mössbauer spectrum of **1b** at 80 K: (−·−) Fe(1,4); (−··−); Fe(2,3); (···) Fe(5).

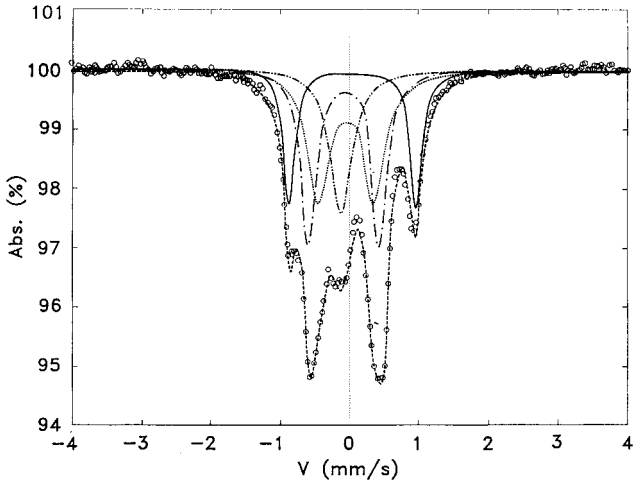

Figure 6. ^{57}Fe Mössbauer spectrum of **1e** at 80 K: (−·−) Fe(1,4); (···) Fe(2,3); (−··−) Fe(5); (−) Fe(6).

Mössbauer Spectroscopy. ^{57}Fe Mössbauer spectroscopy is a relevant technique for the cluster reported here, since it can provide information about the electronic density and asymmetry of the electronic environments of the different iron sites displayed for these species. The Mössbauer spectra of **1b**,**e**, measured at 80 K, are shown in Figures 5 and 6, respectively. The derived spectral hyperfine parameters are given in Table 4.

The structure of $(NEt_4)[Fe_5C(CO)_{14}\{\mu\text{-HgW(CO)}_3\text{Cp}\}]$ (**1b**) shows three types of iron sites: Fe(5) and the chemically equivalent couples Fe(1,4) and Fe(2,3). This observation is in close agreement with its Mössbauer

(22) Gourdon, A.; Jeannin, Y. *J. Organomet. Chem.* **1985**, *290*, 199.
(23) Lemoine, P.; Giraudeau, A.; Gross, M.; Braunstein, P. *J. Chem. Soc., Chem. Commun.* **1980**, 77.
(24) Reina, R.; Rossell, O.; Seco, M.; de Montauzon, D.; Zquiak, R. *Organometallics* **1994**, *13*, 4300.
(25) Rossell, O.; Seco, M.; Segalés, G.; Mathieu, R.; de Montauzon, D. *J. Organomet. Chem.* **1996**, *509*, 241.
(26) Osella, D.; Milone, L.; Kukharenko, S. V.; Strelets, V. V.; Rosenberg, E.; Hajela, S. *J. Organomet. Chem.* **1993**, *451*, 153.
(27) Rossell, O.; Seco, M.; Segalés, G.; Alvarez, S.; Pellinghelli, M. A.; Tiripicchio, A.; de Montauzon, D. *Organometallics* **1997**, *16*, 236.

Table 4. ^{57}Fe Mössbauer Hyperfine Parameters (at 80 K) for Compounds 1b,e

compd	site	IS[a] (δ) (mm s^{-1})	QS (Δ) (mm s^{-1})	line width (mm s^{-1})	rel area (%)
1b	Fe(1,4)	0.07	1.05	0.14	40
	Fe(2,3)	0.09	0.71	0.15	40
	Fe(5)	0.04	0.00	0.16	20
1e	Fe(1,4)	0.05	0.98	0.13	31
	Fe(2,3)	0.08	0.76	0.19	33
	Fe(5)	0.01	0.00	0.18	18
	Fe(6)	0.15	1.74	0.10	18

[a] Isomer shift values referenced to metallic iron at room temperature.

spectrum, which reveals an essentially symmetrical electronic environment for the unique apical Fe(5), as indicated by the absence of a quadrupole interaction for this site. Similar results are found for the unique iron sites in $Fe_3(CO)_{12}$[28] and $(PPN)_2[Fe_4(CO)_{13}]$.[29] The other two signals, the doublet with a small splitting and that with larger quadupole splitting, are assigned to the chemically equivalent Fe(2,3) and Fe(1,4) sites, respectively. This last assignment, which has proved quite difficult in the current work,[30] involved both the evaluation of individual iron site symmetry and the electronic environment at the site. In relation to the latter, the existence of a substantial electric field gradient in some types of iron atoms is known for iron−carbido clusters as a result of the presence of the bonding with the carbide carbon atom.[31] In this sense, the stronger the bond, the larger the gradient will be, though a higher QS value is expected for Fe(1,4) than for Fe(2,3). Moreover, the good agreement of the area ratio 1:2:2 (Fe(5):Fe(1,4):Fe(2,3)) confirms the proposed assignment.

The ^{57}Fe Mössbauer spectrum for complex **1e** deserves special attention. In this anion cluster, we expect to find the not very common feature of four different types of iron sites. This was, in fact, experimentally observed and is shown in Figure 6. The Mössbauer spectrum of this cluster was then fitted with four symmetrical quadrupole doublets with an area ratio of approximately 1:1:2:2. For the assignment of the apical and basal iron atoms we followed the same criterion used for compound **1b**. The last iron site, belonging to the fragment {HgFe(CO)$_2$Cp}, has a quadupole splitting of 1.74 mm s^{-1}. This value compares well with that reported for the compound [Hg{Fe(CO)$_2$Cp}$_2$], QS = 1.6 mm s^{-1}.[32]

In view of these results, although the QS provides a good measure of the asymmetry of the electronic environment around each iron site, we can conclude that in these species the isomer shift has not been as useful as the quadrupole splitting for identifying the iron sites because of the similarity of most IS data.

Experimental Section

All manipulations were performed under an atmosphere of prepurified N_2 with standard Schlenk techniques, and all solvents were distilled from appropriate drying agents. Elemental analyses of C, H, and N were carried out at the Unitat de Cromatografia i Microanàlisi del Servei Científico-Tècnic de la Universitat de Barcelona. Infrared spectra were recorded in THF solutions on an FT-IR 520 Nicolet spectrophotometer. ^{1}H and ^{13}C{^{1}H} NMR spectra were obtained on Bruker DRX 250 and Varian Unity 300 spectrometers (δ(TMS) 0.0 ppm). FABMS and ESMS were recorded in a Fisons VG Quattro spectrometer with methanol as solvent. The compounds ClHgM[33] (M = Mo(CO)$_3$Cp, W(CO)$_3$Cp, Fe(CO)$_2$Cp, Mn(CO)$_5$, Co(CO)$_4$) and $(NEt_4)_2[Fe_5C(CO)_{14}]$[34] were synthesized as previously described.

Synthesis of (NEt$_4$)[Fe$_5$C(CO)$_{14}${μ-HgM}] (M = Mo(CO)$_3$Cp (1a), W(CO)$_3$Cp (1b), Co(CO)$_4$ (1d)). Details of the synthesis of **1a** also apply to **1b** and **1d**. To a precooled suspension of $(NEt_4)_2[Fe_5C(CO)_{14}]$ (0.50 g, 0.53 mmol) in THF (70 mL) at −5 °C was added solid ClHgMo(CO)$_3$Cp (0.52 g, 1.06 mmol). The mixture changed from brown to dark red immediately. After 1 h of stirring, the mixture was filtered off to eliminate NEt_4Cl, and the solution was evaporated to dryness. The residual solid was washed with cooled toluene (15 mL) and dried in vacuo. The remaining product was extracted with methanol (3 × 5 mL) and filtered and the solvent reduced to half-volume. Cooling the solution to −30 °C for 3 h resulted in the deposition of some additional salts (NEt_4Cl). The solution was filtered again, concentrated to 5 mL, and then cooled overnight to −30 °C to obtain 0.43 g (65% yield) of red microcrystals. IR (THF, cm^{-1}): ν(CO) stretch 2053 m, 2010 s, sh, 2000 vs, 1987 vs, 1906 m, 1886 m, 1825 m. ^{1}H NMR (295 K, CD_2Cl_2, δ (ppm)): 5.5 (s, 5H, C_5H_5). ^{13}C NMR (295 K, CD_2Cl_2, δ (ppm)): 481.7 (s, C), 222.3 (br, CO), 216.1 (s, CO), 88.8 (s, C_5H_5). FABS (*m*/*z*): (M^-) 1130, (M − CO) 1102. ESMS (*m*/*z*): (M^-) 1130, (M − CO) 1101. Anal. Calcd: C, 29.55; H, 1.98; N, 1.11. Found: C, 29.15; H, 1.91; N, 1.12. Yield for **1b**: 0.35 g, 50%. IR (THF, cm^{-1}): ν(CO) stretch 2052 m, 2010 s, sh, 1999 vs, 1987 vs, 1892 m, 1879 m, 1822 w. ^{1}H NMR (295 K, CD_2Cl_2, δ (ppm)): 5.6 (s, 5H, C_5H_5). ^{13}C NMR (295 K, CD_2Cl_2, δ (ppm)): 481.2 (s, C), 221.9 (br, CO), 216.2 (s, CO), 87.5 (s, C_5H_5). FABS (*m*/*z*): (M^-) 1217, (M − CO) 1189. ESMS (*m*/*z*): (M^-) 1217, (M − CO) 1189. Anal. Calcd: C, 27.60; H, 1.85; N, 1.04. Found: C, 27.13; H, 1.86; N, 1.02. Yield for **1d**: 0.39 g, 63%. IR (THF, cm^{-1}): ν(CO) stretch 2062 w, sh, 2049 s, 2014 s, sh, 1996 vs, 1826 w. ^{13}C NMR (295 K, CD_2Cl_2, δ (ppm)): 485.7 (s, C), 221.5 (br, CO), 215,7 (s, CO), 206.9 (s, CO). FABS (*m*/*z*): (M^-) 1055, (M − CO) 1026. ESMS (*m*/*z*): (M^-) 1055, (M − CO) 1026. Anal. Calcd: C, 27.35; H, 1.69; N, 1.18. Found: C, 27.13; H, 1.73; N, 1.21.

Synthesis of (NEt$_4$)[Fe$_5$C(CO)$_{14}${μ-HgMn(CO)$_5$}] (1c). The general procedure described above also applies for **1c**, but in this case a 10% excess of ClHgMn(CO)$_5$ was used. Yield: 0.25 g, 40%. IR (THF, cm^{-1}): ν(CO) stretch 2081 w, 2046 m, 2011 m, 1994 vs, 1826 w. ^{13}C NMR (295 K, CD_2Cl_2, δ (ppm)): 481.4 (s, C), 217.5 (br, CO), 217.3 (s, CO), 213.9 (s, CO). FABS (*m*/*z*): (M^-) 1079, (M − CO) 1051. ESMS (*m*/*z*): (M^-) 1078, (M − CO) 1051. Anal. Calcd: C, 27.80; H, 1.65; N, 1.16. Found: C, 28.50; H, 1.71; N, 1.22.

Synthesis of (NEt$_4$)[Fe$_5$C(CO)$_{14}${μ-HgFe(CO)$_2$Cp}] (1e). The general procedure described above also applies for **1e**, but in this case a 70% excess of ClHgFe(CO)$_2$Cp was used. Yield: 0.34 g, 55%. IR (THF, cm^{-1}): ν(CO) stretch 2049 m, 2010 s, sh, 1997 s, 1984 vs, 1957 m, 1924 m, 1820 w. ^{1}H NMR (295 K, CD_2Cl_2, δ (ppm)): 4.9 (s, 5H, C_5H_5). ^{13}C NMR (295 K, CD_2Cl_2, δ (ppm)): 480.1 (s, C), 223.0 (br, CO), 217.1 (s, CO), 212.7 (s, CO), 80.8 (s, C_5H_5). FABS (*m*/*z*): (M^-) 1061, (M − CO) 1033.

(28) Benson, C. G.; Long, G. J.; Kolis, J. W.; Shriver, D. F. *J. Am. Chem. Soc.* **1985**, *107*, 5297.
(29) Benson, C. G.; Long, G. J.; Bradley, J. S.; Kolis, J. W.; Shriver, D. F. *J. Am. Chem. Soc.* **1986**, *108*, 5297.
(30) For reasons unknown the hyperfine parameters of the iron clusters studied in this work do not compare well with those of the related compounds $[Fe_5C(CO)_{15}]$ and $[Fe_5C(CO)_{14}]^{2-}$: Brint, R. P.; O'Cuill, K.; Spalding, T. R.; Deeny, F. A. *J. Organomet. Chem.* **1983**, *247*, 61. Brint, R. P.; Collins, M. P.; Spalding, T. R.; Deeny, F. A. *J. Organomet. Chem.* **1983**, *258*, C57.
(31) (a) Buhl, M. L.; Long, G. J.; O'Brien, J. F. *Organometallics* **1993**, *12*, 283. (b) Buhl, M. L.; Long, G. J.; O'Brien, J. F. *Organometallics* **1993**, *12*, 1902 and references therein.
(32) Greenwood, N. N.; Gibb, T. C. *Mössbauer Spectroscopy*; Chapman and Hall: London, 1971.
(33) Mays, M. J.; Robb, J. D. *J. Chem. Soc. A* **1968**, 329.
(34) Tachikawa, M.; Geerts, R. L.; Muetterties, E. L. *J. Organomet. Chem.* **1981**, *213*, 11.

Table 5. Crystal Data and Structure Refinement Details for Compounds 1b and 2

compd	**1b**	**2**
empirical formula	$C_{31}H_{25}Fe_5HgNO_{17}W\cdot{}^1/_2C_4H_{10}O$	$C_{46}H_{40}Fe_{10}HgN_2O_{28}\cdot{}^1/_2CH_2Cl_2$
fw	1347.21	1870.35
temp (K)	293(2)	
wavelength (Å)	0.710 73	
cryst syst	triclinic	monoclinic
space group	$P\bar{1}$	$P2_1/n$
unit cell dimens	a = 8.648(2) Å	a = 15.604(1) Å
	b =15.258(3) Å	b = 14.344(1) Å
	c =17.930(4) Å	c = 29.930(1) Å
	α =110.54(3)°	α = 90°
	β =97.50(3)°	β = 104.05(1)°
	γ =101.99(3)°	γ = 90°
V (Å^3)	2113.0(8)	6498.6(7)
Z	2	4
density (calcd) (g/cm^3)	2.117	1.912
abs coeff (mm^{-1})	8.064	4.634
F(000)	1276	3660
cryst size (mm)	0.40 × 0.25 × 0.22	0.41 × 0.36 × 0.32
θ range for data collection (deg)	2.28−24.97	3.04−23.00
index ranges	$-10 < H < 10$, $-18 < K < 18$, $0 < L < 21$	$-17 < H < 16$, $0 < K < 15$, $0 < L < 32$
no. of rflns collected	7818	9644
no. of indep rflns	7425 (R_{int} = 0.0167)	9014 (R_{int} = 0.261)
no. of obsd rflns ($I > 2\sigma(I)$)	6080	5540
abs cor	ψ scan	ψ scan
max and min transmissn	1.000 and 0.260	0.304 and 0.230
refinement method	full-matrix least squares on F^2	
no. of data/restraints/params	7414/0/478	9014/0/801
goodness of fit on F^2	1.088	1.065
final R indices ($I > 2\sigma(I)$)	R1 = 0.0440, wR2 = 0.1139	R1 = 0.0980; wR2 = 0.2512
R indices (all data)	R1 = 0.0711, wR2 = 0.1524	R1 = 0.1540; wR2 = 0.2884
weighting scheme (calcd)[a]	$w = 1/[\sigma^2(F_o^2) + (0.0739P)^2 + 10.2649P]$	$w = 1/[\sigma^2(F_o^2) + (0.2000P)^2]$
largest diff peak and hole (e/Å^3)	1.996 and −1.746	3.868 and −3.736 (∼1 Å from Hg)

[a] $P = (F_o^2 + 2F_c^2)/3$.

ESMS (m/z): (M^-) 1060, (M − CO) 1033. Anal. Calcd: C, 30.23; H, 2.10; N, 1.17. Found: C, 29.60; H, 2.12; N, 1.12.

Synthesis of $(NEt_4)_2[\mu_4$-Hg$\{Fe_5C(CO)_{14}\}_2]$ (2). Solid $Hg(NO_3)_2$ (0.16 g, 0.46 mmols) was added to a suspension of $(NEt_4)_2[Fe_5C(CO)_{14}]$ (1.00 g, 1.06 mmol) in THF (70 mL). The solution was stirred at room temperature for 5 h and then filtered and evaporated to dryness. The residual solid was washed with cooled toluene (15 mL) and extracted with 15 mL of methanol. The solution obtained was concentrated to half-volume and cooled overnight at −30 °C. Red crystals of $(NEt_4)_2[\mu_4$-Hg$\{Fe_5C(CO)_{14}\}_2]$ were obtained (0.50 g, 60% yield). IR (THF, cm^{-1}): ν(CO) stretch 2038 m, 2009 vs, 1995 s, sh, 1989 s, sh, 1820 w. ^{13}C NMR (295 K, CD_2Cl_2, δ (ppm)): 482.3 (s, C), 480.8 (s, C), 228.2 (br, CO), 216.6 (s, CO), 215.8 (s, CO). FABS (m/z): (M + H$^-$) 1568. ESMS (m/z): (M/2) 783. Anal. Calcd: C, 30.20; H, 2.18; N, 1.53. Found: C, 29.27; H, 2.25; N, 1.47.

Synthesis of $[Fe_5C(CO)_{14}\{\mu$-HgM$\}\{\mu_4$-AuPPh$_3\}]$ (M = Mo(CO)$_3$Cp (3a), W(CO)$_3$Cp (3b)). Details of the synthesis of **3b** also apply to **3a**. Solid $ClAuPPh_3$ (0.23 g, 0.47 mmol) and $TlBF_4$ (0.14 g, 0.47 mmol) were added to a solution of $(NEt_4)[Fe_5C(CO)_{14}\{\mu$-HgW(CO)$_3Cp\}]$ (0.63 g, 0.47 mmol) in CH_2Cl_2 (60 mL) at room temperature. The solution was stirred for 1 h, and 30 mL of diethyl ether was added. After the solution was filtered off, the solvent was evaporated in vacuo. The product was extracted with toluene (3 × 10 mL) and the solution was concentrated to 10 mL. After the solution was layered with hexane (20 mL) and cooled overnight (−30 °C), dark brown crystals of $[Fe_5C(CO)_{14}\{\mu$-HgW(CO)$_3$Cp$\}\{\mu_4$-AuPPh$_3\}]$ were obtained (yield 0.40 g, 51%). IR (KBr, cm^{-1}): ν(CO) stretch 2069 m, 2024 s, sh, 2007 vs, 1992 s, 1970 vs, 1942 m, 1875 m, 1834 m, 1820 m. ^{1}H NMR (295 K, CD_2Cl_2, δ (ppm)): 7.3 (m, 15H, C_6H_5), 5.6 (s, 5H, C_5H_5). ^{13}C NMR (295 K, CD_2Cl_2, δ (ppm)): 134.2−129.1 (m, C_6H_5) 219.2 (br, CO), 216.1 (s, CO), 87.8 (s, C_5H_5). ^{31}P NMR (295 K, CH_2Cl_2, δ (ppm)): 33.4 (s, PPh$_3$). FABMS (m/z): (M^-) 1676, (M − CO) 1648, (M − 2CO) 1620. Anal. Calcd: C, 29.36; H, 1.19. Found: C, 29.72; H, 1.21. Yield for **3a**: 0.35 g, 44%. IR (KBr, cm^{-1}): ν(CO) stretch 2069 m, 2027 s, sh, 2008 vs, 1991 s, 1977 vs, 1943 m, 1881 m, 1835 m, 1822 m. ^{1}H NMR (295 K, CD_2Cl_2, δ (ppm)): 7.3 (m, 15H, C_6H_5), 5.5 (s, 5H, C_5H_5). ^{13}C NMR (295 K, CD_2Cl_2, δ (ppm)): 133.7−129.5 (m, C_6H_5), 221.9 (br, CO), 212.2 (s, CO), 89.5 (s, C_5H_5). ^{31}P NMR (295 K, CH_2Cl_2, δ (ppm)): 33.3 (s, PPh$_3$). FABMS (m/z): (M^-) 1587, (M − CO) 1559, (M − 2CO) 1531. Anal. Calcd: C, 30.99; H, 1.26. Found: C, 31.19; H, 1.30.

Electrochemical Measurements. Electrochemical measurements were carried out with an Electrokemat potentiostat[35] using the interrupt method to minimize the uncompensated resistance (iR) drop. Electrochemical experiments were performed at room temperature in an airtight three-electrode cell connected to a vacuum argon/N_2 line. The reference electrode consisted of a saturated calomel electrode (SCE) separated from the nonaqueous solutions by a bridge compartment. The counter electrode was a spiral of ca. 1 cm^2 apparent surface area, made of a platinum wire 8 cm in length and 0.5 cm in diameter. The working electrode was Pt (1 mm diameter) for cyclic voltammetry or a rotating-disk electrode of Pt of 2 mm diameter for linear voltammetry. For electrolysis a Pt foil was used. $E^{o\prime}$ values were determined as the average of the cathodic and anodic peak potentials, i.e. $(E_{p,c} + E_{p,a})/2$. The supporting electrolyte (n-Bu$_4$N)[PF_6] (Aldrich analytical grade) was used as received. Dichloromethane (SDS purex) was freshly distilled over $CaCl_2$ and then over P_2O_5 prior to use. The solutions used during the electrochemical studies were typically 4 × 10^{-4} M in the organometallic complex and 0.1 M in (n-Bu$_4$N)[PF_6]. Under the same conditions, ferrocene is oxidized at $E^{o\prime}$ = 0.42 V vs SCE and the peak potential separation ΔE is 60 mV.

Computational Details. The extended Hückel calculations were carried out using the program CACAO.[36] The

(35) Cassoux, P.; Dartiguepeyron, R.; de Montauzon, D.; Tommasino, J. B.; Fabre, P. L. *Actual. Chim.* **1994**, *1*, 49.

(36) Mealli, C.; Proserpio, D. M. Computer Aided Composition of Atomic Orbitals, CACAO Program, Version 4.0, 1994. *J. Chem. Educ.* **1990**, *67*, 399.

molecular orbitals (MO) were built using the fragments $[Fe_5C(CO)_{14}]^{2-}$ and $\{HgW(CO)_3Cp\}^+$ or $\{AuPH_3\}^+$ (as a simplification of $AuPPh_3$).[37] The model $[Fe_5C(CO)_{14}]^{2-}$ was constructed with the distances and angles of the $[Fe_5C(CO)_{14}\{\mu\text{-}HgW(CO)_3Cp\}]^-$ anion, the X-ray structure of which is reported herein. The position of the terminal CO ligands has been idealized in order to allow all the calculated species to be compared. The distances Fe−Au (μ_2 and μ_4) used were those found in the literature. For the hypothetical geometries the distances Fe−Hg and Fe−Au were assumed to be the same.

Mössbauer Measurements. The Mössbauer spectra were recorded in a transmission geometry using driving equipment of constant acceleration provided by a ^{57}Co (50 mCi) source diffused into a Rh matrix and was calibrated at room temperature with natural-abundance α-iron foil. The measurements were carried out at 80 K using an MD 306 Oxford cryostat. The spectra were fitted to symmetrical Lorentzian doublets by using standard least-squares computer minimization techniques.[38]

X-ray Structure Determination of 1b and 2. Red block crystals of compounds **1b** and **2** were mounted in glass capillaries in a random orientation on an Enraf-Nonius CAD-4 four-circle automatic diffractometer with graphite-monochromated Mo Kα radiation ($\lambda = 0.7073$ Å). Crystallographic and experimental details of both compounds are summarized in Table 5. Compound **1b** crystallizes with a disordered molecule of diethyl ether with the oxygen atom located on a center of symmetry, while compound **2** crystallizes with a molecule of dichloromethane which is refined only with half-occupancy. Data were collected at room temperature. Intensities were corrected for Lorentz and polarization effects in the usual manner. Absorption corrections were carried out by ψ-scan methods. Intensity measurements were performed by $\omega-2\theta$ scans.

The structures were solved by direct methods (SHELXS-90)[39] and refined by least squares against F^2 (SHELXL-93).[40] Details of refinement parameters are included in Table 5. The values of R1 and wR2 are defined as $R1 = \sum||F_o| - |F_c||/[\sum|F_o|]$ and $wR2 = \{[\sum w(F_o^2 - F_c^2)^2]/[\sum w(F_o^2)^2]\}^{1/2}$, and σ was obtained from counting statistics. All non-hydrogen atoms were refined anisotropically, except for the carbon atoms of the tetraethylamonium cation (slightly disordered, largest peak in the difference map was located 1.566 Å from the nitrogen atom) and those corresponding to the disordered solvent (50% occupancies) in **1b**. In compound **2** only two carbon atoms were isotropically refined, and the largest peak in the difference map appeared close to the Hg atom. The hydrogen atoms were introduced in the last cycle of refinement from geometrical calculations where possible and refined using a riding model with thermal parameters fixed at $U = 0.08$ Å^2.

Acknowledgment. Financial support for this work was generously given by the DGICYT (Project PB96-0174) and Universidad de Alcalá (Project E001/97) and by the CIRIT (Project 1997SGR 00174).

Supporting Information Available: Tables giving experimental details of X-ray structural determinations, final values of atomic coordinates for the non-hydrogen atoms, calculated coordinates and isotropic thermal parameters for the hydrogen atoms, anisotropic thermal parameters for the non-hydrogen atoms, and all bond distances and angles (15 pages). Ordering information is given on any current masthead page.

OM9801608

(37) Calculations were carried out with $\{AuPH_3\}^+$ instead of $\{AuPPh_3\}^+$, for simplicity. In fact, the gold sp, p_x, and p_y orbitals of this latter fragment are only 0.1 eV less stable than those of the $\{AuPH_3\}^+$ group.

(38) Varret, F. *Proceedings of the International Conference on Mössbauer Effect Application*; Jaipur, India, 1981; Indian National Science Academy: New Delhi, 1982.

(39) Sheldrick, G. M. *Acta Crystallogr., Sect. A* **1990**, *46*, 467.

(40) Sheldrick, G. M. SHELXL 93; University of Gottingen, Gottingen, Germany, 1993 (PC version).